Arteriosclerosis, Thrombosis, and Vascular Biology

ORIGINAL RESEARCH

Single-Molecule Spatial Transcriptomics of Human Thoracic Aortic Aneurysms Uncovers Calcification-Related *CARTPT*-Expressing Smooth Muscle Cells

Dogukan Mizrak,* Yang Zhao,* Hao Feng, Jane Macaulay, Ying Tang, Zain Sultan, Guizhen Zhao, Yanhong Guo, Jifeng Zhang, Bo Yang, Y. Eugene Chen

BACKGROUND: Although single-cell RNA-sequencing is commonly applied to dissect the heterogeneity in human tissues, it involves the preparation of single-cell suspensions via cell dissociation, causing loss of spatial information. In this study, we employed high-resolution single-cell transcriptome imaging to reveal rare smooth muscle cell (SMC) types in human thoracic aortic aneurysm (TAA) tissue samples.

METHODS: Single-molecule spatial distribution of transcripts from 140 genes was analyzed in fresh-frozen human TAA samples with region and sex-matched controls. In vitro studies and tissue staining were performed to examine human CART prepropeptide (*CARTPT*) regulation and function.

RESULTS: We captured thousands of cells per sample including a spatially distinct *CARTPT*-expressing SMC subtype enriched in male TAA samples. Immunoassays confirmed human CART enrichment in male TAA tissue and truncated CARTPT secretion into cell culture medium. Oxidized low-density lipoprotein, a cardiovascular risk factor, induced *CARTPT* expression, whereas *CARTPT* overexpression in human aortic SMCs increased the expression of key osteochondrogenic transcription factors and reduced contractile gene expression. Recombinant human CART treatment of human SMCs further confirmed this phenotype. Alizarin red staining revealed calcium deposition in male TAA samples showing similar localization with human CART staining.

CONCLUSIONS: Here, we demonstrate the feasibility of single-molecule imaging in uncovering rare SMC subtypes in the diseased human aorta, a difficult tissue to dissociate. We identified a spatially distinct *CARTPT*-expressing SMC subtype enriched in male human TAA samples. Our functional studies suggest that human CART promotes osteochondrogenic switch of aortic SMCs, potentially leading to medial calcification of the thoracic aorta.

Key Words: aorta ■ aortic aneurysm, thoracic ■ gene expression profiling ■ myocytes, smooth muscle ■ risk factors

Thoracic aortic aneurysm (TAA) is a major cause of morbidity and mortality in the United States. Surgical repair is still the standard TAA treatment due to the inadequate understanding of human TAA pathogenesis and lack of alternative therapeutics. The human aorta harbors multiple cell types, and vascular smooth muscle cells (SMCs) of different developmental origins are the predominant cell type forming the vascular wall. SMC defects are the major determinant of aortic diseases and regional TAA susceptibility has been

Nonstandard Abbreviations and Acronyms

CARTPT	CART prepropeptide
ERK	phosphorylated-ERK
MERFISH	multiplexed error-robust fluorescence in situ hybridization
oxLDL	oxidized low-density lipoprotein
qPCR	quantitative polymerase chain reaction
rhCART	recombinant human CART
rhTNFα	recombinant human TNF-alpha
scRNA	single-cell RNA-sequencing
SMC	smooth muscle cell
TAA	thoracic aortic aneurysm
TNF	tumor necrosis factor

Highlights

- Single-molecule spatial transcriptomics is a powerful method to begin to characterize tissue-resident human aortic cell heterogeneity.
- We identified a spatially distinct *CARTPT*-expressing smooth muscle cell subtype predominantly found in male thoracic aortic aneurysm tissue.
- Functional studies suggest that human CART promotes osteochondrogenic differentiation of aortic smooth muscle cells, potentially leading to medial calcification of the thoracic aorta.

linked to lineage-specific SMC dysfunction.[1–7] Given the significant genetic and regional heterogeneity of human TAAs, high-resolution approaches are required to reveal the SMC defects underlying TAA initiation and progression.[7,8]

Single-cell RNA-sequencing (scRNA-seq) is frequently employed to resolve cell heterogeneity in healthy and diseased human tissue. However, scRNA-seq involves the preparation of single-cell suspensions which causes gene expression changes and loss of spatial information. The human aorta is particularly difficult to dissociate due to its high extracellular matrix content. Despite this challenge, many single-cell genomics studies provided key insights into the SMC subtypes in the aneurysmal human aorta.[9–11] Spatial transcriptomics is a powerful alternative to scRNA-seq as it enables gene expression measurements in native tissue context. Particularly, in situ hybridization–based spatial profiling strategies including multiplexed error-robust fluorescence in situ hybridization (MERFISH) offer near single-molecule sensitivity and high spatial resolution in fresh-frozen tissue preparations, representing an ideal tool to study human aortic heterogeneity.[12] To date, high-resolution, multiplexed spatial profiling technologies have not been applied to investigate human TAA, leaving the spatial remodeling in human TAA tissue including disease-causing and protective changes unexplored.

In this study, we demonstrate the feasibility of MERFISH profiling of the human aorta for the first time, revealing the spatial organization of rare SMC subtypes in human TAA. This platform enabled us to uncover a spatially distinct SMC subtype marked by CART prepropeptide (*CARTPT*) expression. We present functional evidence that human CART promotes the expression of osteochondrogenic switch markers in human SMCs and is likely a potentiator of medial calcification in male human TAA samples.

METHODS

All experiments were performed according to the protocols (HUM00035836, HUM00096079, HUM00054585, and HUM00052866) approved by the Institutional Review Board at the University of Michigan. The study materials can be made available from the corresponding authors on reasonable request. Single-cell MERSCOPE data are deposited to the Gene Expression Omnibus database under the accession number GSE241870. Detailed descriptions of the reagents are in the Major Resources Table.

MERFISH Profiling and Single-Cell Data Analysis

Surgically resected fresh ascending aorta samples from 2 control subjects with no aortic aneurysms (denoted as ♂Control and ♀Control) and 3 TAA subjects (denoted as ♂TAA1, ♂TAA2, and ♀TAA1) with ascending aneurysms were immediately embedded and frozen in optimal cutting temperature compound (Catalog No. 23-730-571; Fisher). All tissue samples were extracted from the greater curvature of the ascending aorta for a proper comparison. Age, sex, race, aneurysm size, disease condition, and smoking status of each subject are indicated in Table S1. RNA quality of each sample was assessed using Agilent Bioanalyzer (RNA integrity number >7) before processing the samples. Optimal cutting temperature compound–embedded ascending aorta samples were cut into 10-µm sections using a cryostat and adhered onto the imageable area of Vizgen slides. Immediately after removing the slides from the cryostat, they were fixed in preheated 4% paraformaldehyde for 30 minutes at 47 °C. Subsequent slide processing was performed according to fresh-frozen tissue preparation protocol by Vizgen. Hybridization of custom MERFISH probes targeting 140 genes, gel embedding, and tissue clearing were performed by Vizgen according to the MERSCOPE User Guide. Each sample was stained with both DAPI and Poly(T) staining reagents.

Cell segmentation boundaries were determined using the default MERFISH approach.[12] The Vizgen MERSCOPE data (1 intact tissue segment per sample) and cell boundaries were inputted to Seurat 4.2 (R package) using LoadVizgen function.[13] Cells with <20 molecules were discarded from the subsequent analysis. SCTransform and ScaleData functions of Seurat were used to normalize and scale the data respectively. Unsupervised clustering (Louvain algorithm) and dimensionality reduction were

performed using Seurat to identify spatially resolved cell types on the merged dataset of 2 control and 3 TAA samples. FeaturePlot and ImageFeaturePlot functions were executed to visualize the data on a 2-dimensional embedding. ImageDimPlot function was used to visualize the localization of individual molecules. Cluster markers were identified using PrepSCTFindMarkers and FindAllMarkers functions, respectively. Differential gene expression comparing control and TAA samples were performed using FindMarkers function, which uses Wilcoxon Rank-Sum test. P value adjustment is performed using Bonferroni correction.

The MERSCOPE data was compared with human TAA scRNA-seq data set generated by Li et al.[9] The scRNA-seq expression matrices were downloaded from Gene Expression Omnibus dataset under GSE155468 (https://www.ncbi.nlm.nih. gov/geo/query/acc.cgi?acc=GSE155468). Three controls (ages 61−63 years old), 3 male TAA samples (ages 56−69 years old), and 3 female TAA samples (ages 67−75 years old) were inputted to Seurat 4.2 (R package). We excluded TAA subjects with bicuspid aortic valve to be consistent with our MERSCOPE TAA samples. The single cells with >1000 molecule count and less than 10% mitochondrial content were kept for the subsequent analysis. The resulting samples were merged using IntegrateData function and clustered using Seurat. Cluster markers were identified using FindAllMarkers function and SMC clusters were identified based on significant $MYH11$ enrichment (fold-change >2.0, adjusted P value [P-adj] <0.001) in the merged dataset.

Immunohistochemistry, Alizarin Red, and von Kossa Stainings

Immunohistochemical analysis was conducted using Abcam ab64264 kit. Paraffin blocks were prepared from 2 control (non-aneurysmal) subjects independent of the MERSCOPE control subjects, 4 male TAA subjects (including ♂TAA1 and ♂TAA2), and 4 female TAA subjects (including ♀TAA1). The blocks were sectioned to a thickness of 5 μm and then deparaffinized. After rehydration, the samples underwent antigen retrieval using citrate buffer in a pressure cooker for 15 minutes. After cooling completely, the tissue sections were washed 4 times in TBS and treated with a hydrogen peroxide−blocking solution for 10 minutes. Following 2 washes with TBS, the tissue sections were incubated at room temperature for 10 minutes in Protein blocking solution. Subsequently, the tissue sections were incubated in CART antibody (Catalog No. 14437, 1:75; Cell Signaling Technology) in 1% BSA overnight at 4 °C. After the primary antibody incubation, the sections underwent 4 TBS washes and were then incubated with a biotinylated secondary antibody for 30 minutes. The tissue sections were then washed 4 additional times in TBS and streptavidin peroxidase was applied to the sections for 30 minutes. Following 4 TBS washes, the slides were incubated with DAB Chromogen and DAB substrate (1:30) for 1 minute. A counterstain of Hematoxylin was applied, and the slides were imaged using a KEYENCE microscope (BZ-X810).

For Alizarin red staining, the paraffin-embedded tissue specimens were sectioned into 4 μm thick slices. After deparaffinization and hydration, the samples were covered in an Alizarin Red staining solution (Catalog No. TMS-008-C; Sigma) and incubated for 30 minutes at room temperature. Subsequently, the slides were washed in PBS before dehydrating in Acetone and then in an Acetone-Xylene (1:1) solution for 40 seconds in each. The slides were then soaked in xylene for a minute twice before

mounting. For von Kossa staining, paraffin blocks were sectioned to a thickness of 5 μm, deparaffinized, and rehydrated. The sections were incubated in 5% Silver nitrate solution (Catalog No. S8157; Sigma) for 1 hour under ultraviolet light. Following 2 washes in Milli-Q water (3 minutes each), the sections were covered in 2% Sodium Thiosulphate (Catalog No. 72049; Sigma) for 5 minutes. Following 2 additional washes in Milli-Q water, the sections were counterstained with Eosin (7111 L; Fisher), dehydrated, and cleared. The sections were imaged using a KEYENCE microscope (BZ-X810) and analyzed with ImageJ.

CARTPT Induction, Overexpression, and Recombinant Human CART Treatment

Primary aortic SMCs were isolated from the thoracic aorta, as previously described.[14,15] Cells were cultured in DMEM/ Nutrient Mixture F12 (DMEM/F12; Catalog No. 11330-057; Gibco), supplemented with 20% FBS and 1% penicillin-streptomycin before the cell culture experiments. To ensure consistency in cellular behavior and integrity, primary SMCs from the same passage were used in nontreatment and treatment conditions. For the induction of *CARTPT* expression, a healthy male donor (with no aortic aneurysm) primary SMCs (passage 4) were cultured in DMEM/F12, supplemented with 10% FBS and 1% penicillin-streptomycin, until 70% to 80% confluence was reached. Cells were then stimulated for 16 hours using either a vehicle control, 10 ng/mL rhTNFα (recombinant human TNF [tumor necrosis factor]-alpha; Catalog No. 210-TA-100; Fisher), or 25 μg/mL oxLDL (oxidized low-density lipoprotein). The oxLDL was freshly prepared through copper catalysis of native human plasma LDL (Catalog No. L3486; Fisher) for 4 hours at 37 °C, followed by dialysis against PBS. Subsequently, mRNA was extracted for further analysis. *CARTPT* overexpression experiments were performed by culturing the healthy donor primary SMCs (passage 4) overnight in DMEM/F12, supplemented with 10% FBS and 1% penicillin-streptomycin until ≈60% confluence was achieved. Cells were then washed with PBS and transfected with either 1 μg/mL of control *pcDNA 3.1, pRP[Exp]-CMV>EGFP-EF1A>human CARTPT* (Vectorbuilder, used for real-time quantitative polymerase chain reaction [qPCR]) or *p-CMV3-CARTPT-HA* (Catalog No. HG13240-CY, used for coimmuniprecipitation; Sino Biological) vectors. Transfection was carried out for an additional 48 hours in serum-reduced OPTI-MEM (Catalog No. 31985070; Gibco) using Lipofectamine 2000 (Catalog No. 1668019; Invitrogen) following the manufacturer's protocol. Post-transfection, DNase-digested mRNA and protein were extracted, and conditioned media were collected for further analysis. For recombinant CART treatment, the healthy donor primary SMCs were cultured overnight in DMEM/F12 supplemented with 10% FBS and 1% penicillin-streptomycin until ≈60% confluence was achieved. Subsequently, the cells were treated with either rhCART (recombinant human CART; Catalog No. 10974-CO-050; R&D) or control 4 mM HCl for 0 to 48 hours, following a decreasing order. On completion of the treatment, mRNA and protein were harvested.

RNA Extraction and Quantitative Real-Time PCR

For RNA extraction, we used the RNeasy Mini Kit to directly isolate mRNA from the cells. The isolated mRNA was

reverse-transcribed into cDNA using the SuperScript III kit (Catalog No. 18080051; Fisher), as per the manufacturer's instructions, and utilizing random hexamers to prime the reaction. To quantify the relative abundance of cDNA, the BioRad Real-Time PCR Detection System was employed, using the SYBR Green Fast qPCR Mix (Catalog No. RK21203; Abclonal) for fluorescence detection. Gene expression levels were quantified using the $2^{-\Delta\Delta Ct}$ method, with *GAPDH* serving as the internal control for normalization. The primer sequences used for each target gene in the qPCR analyses are listed in the Major Resources Table. All real-time qPCRs were conducted on primary SMCs from independent rounds of treatments, and matching control and experimental samples were collected from each round of treatment.

Western Blotting and Coimmunoprecipitation

Cells were lysed using Radioimmunoprecipitation Assay buffer (Catalog No. 89901; Fisher), supplemented with protease inhibitor cocktail (Catalog No. 11873580001; Roche) and PhosSTOP phosphatase inhibitors (Catalog No. 4906845001; Roche). The resultant protein extracts were subjected to SDS-PAGE for resolution and then transferred onto nitrocellulose membranes. Membranes were blocked with 5% nonfat milk for 1 hour at room temperature. Subsequently, they were incubated with the 1:1000 diluted p-ERK (phosphorylated-ERK; Catalog No. 4370; CST) and ERK (Catalog No. 9102; CST) primary antibodies overnight at 4 °C, followed by a 1-hour incubation at room temperature with the fluorescence-conjugated secondary antibody (1:4000; Li-Cor Bioscience). The membrane was then scanned using the LI-COR DLx Odyssey imaging system. Protein bands were quantified using the LI-COR Empiria Studio software. For coimmunoprecipitation studies, conditioned media were centrifuged at 500*g* for 10 minutes to remove cellular debris. The supernatants were then immunoprecipitated using Protein G Magnetic Beads (Catalog No. 7024; CST) in conjunction with either IgG control or HA-targeting antibody (Catalog No. 3724; CST), following the manufacturer's protocol. Eluted samples were further concentrated by evaporating at 65 °C. Western blotting was then conducted using primary antibody against CART (Catalog No. 14437; CST). All Western blots were conducted on primary SMCs from independent rounds of treatments, and matching control and experimental samples were collected from each round of treatment.

Statistical Analysis for Cell Culture Experiments

The cell culture experiments were performed on at least 6 replicates and the quantitative cell culture data were presented as mean±SD. When analyzing 2 datasets that are normally distributed (Shapiro-Wilk normality test), we performed 2-tailed unpaired *t* test. If the variances are significantly different (*F* test), we used 2-tailed unpaired *t* test with Welch correction. When analyzing 2 datasets that are not normally distributed, we used nonparametric 2-tailed Mann-Whitney *U* test. When analyzing >2 groups that are not normally distributed, we performed nonparametric Kruskal-Wallis test with Dunn multiple comparisons test. Individual *P* values are presented in the figures up to the significance level $P<0.0001$ and $P \le 0.05$ was considered statistically significant. The statistical analyses were performed using GraphPad Prism 9 Software.

RESULTS

Single-Molecule Spatial Transcriptomics of Human TAA Tissue

We analyzed the single-molecule spatial distribution of transcripts from 140 aortic cell heterogeneity and aneurysm-related genes plus signaling pathways on 2 control samples (♂Control, ♀Control) without aortic aneurysm and 3 TAA samples with ascending aneurysm (Ascending aorta measurements: ♂TAA1=5.0 cm, ♂TAA2=5.6 cm, ♀TAA1=6.0 cm) using the MERSCOPE platform (Figure 1A; Table S1).[7–9,11,16–31] The complete list of genes in the panel are listed in Supplemental Excel Sheet 1. Optimal cutting temperature compound–embedded ascending aorta samples were cut into 10-µm sections and processed using optimized conditions for human aortic tissue. Of note, when the aorta is sliced into smaller pieces, it bends towards adventitia, positioning adventitia in the inner curve and intima in the outer curve (Figure 1A). Overall transcript/molecule detection efficiency per field of view was consistent between different samples (Figure 1B). Cell segmentation was able to capture thousands of single cells per sample; (♂Control: 6753 cells, ♀Control: 10172 cells, ♂TAA1: 19767 cells, ♂TAA2: 16430 cells, ♀TAA1: 15882 cells; Figure 1A).[12] The segmented cells had similar individual cell volume distribution across different samples (Figure 1C). MERFISH-derived single-cell expression profiles were analyzed using Seurat 4.2 (R package) extension for MERSCOPE system.[13]

Unsupervised clustering revealed 3 distinct cell clusters in addition to SMC clusters constituting the aortic media, and the major clusters contained contributions from each sample (Figure 1D). SMC clusters were further subclustered in Figure 2. Fibroblast cluster was enriched in coiled-coil domain containing 80 (*CCDC80*), podocan (*PODN*), and serpin family F member1 (*SERPINF1*; fold-change >2, *P*-adj<0.001; Supplemental Excel Sheet 2); immune cell cluster in membrane-spanning 4-domains A7 (*MS4A7*) and Fc epsilon receptor Ig (*FCER1G*; fold-change >2, *P*-adj<0.001, Supplemental Excel Sheet 2); and endothelial cell cluster in platelet/endothelial cell adhesion molecule 1 (*PECAM1*) and von Willebrand factor (*VWF*; fold-change >2, *P*-adj<0.001, Supplemental Excel Sheet 2; Figure 1E). We also examined the spatially resolved expression of cluster markers showing that SMC markers dominate the aortic media while fibroblast, immune cell, and endothelial cell cluster markers were located in the adventitia and intima layers (Figure 1F). Endothelial cells were present both in the aortic intima and adventitial microvessels (Figure 1G). Among the fibroblast markers, individual *CCDC80* molecules were more restricted to the adventitia, whereas *PODN* molecules also showed localization in the intima, implying additional fibroblast heterogeneity consistent with the previous reports (Figure 1G).[9] Next, we analyzed
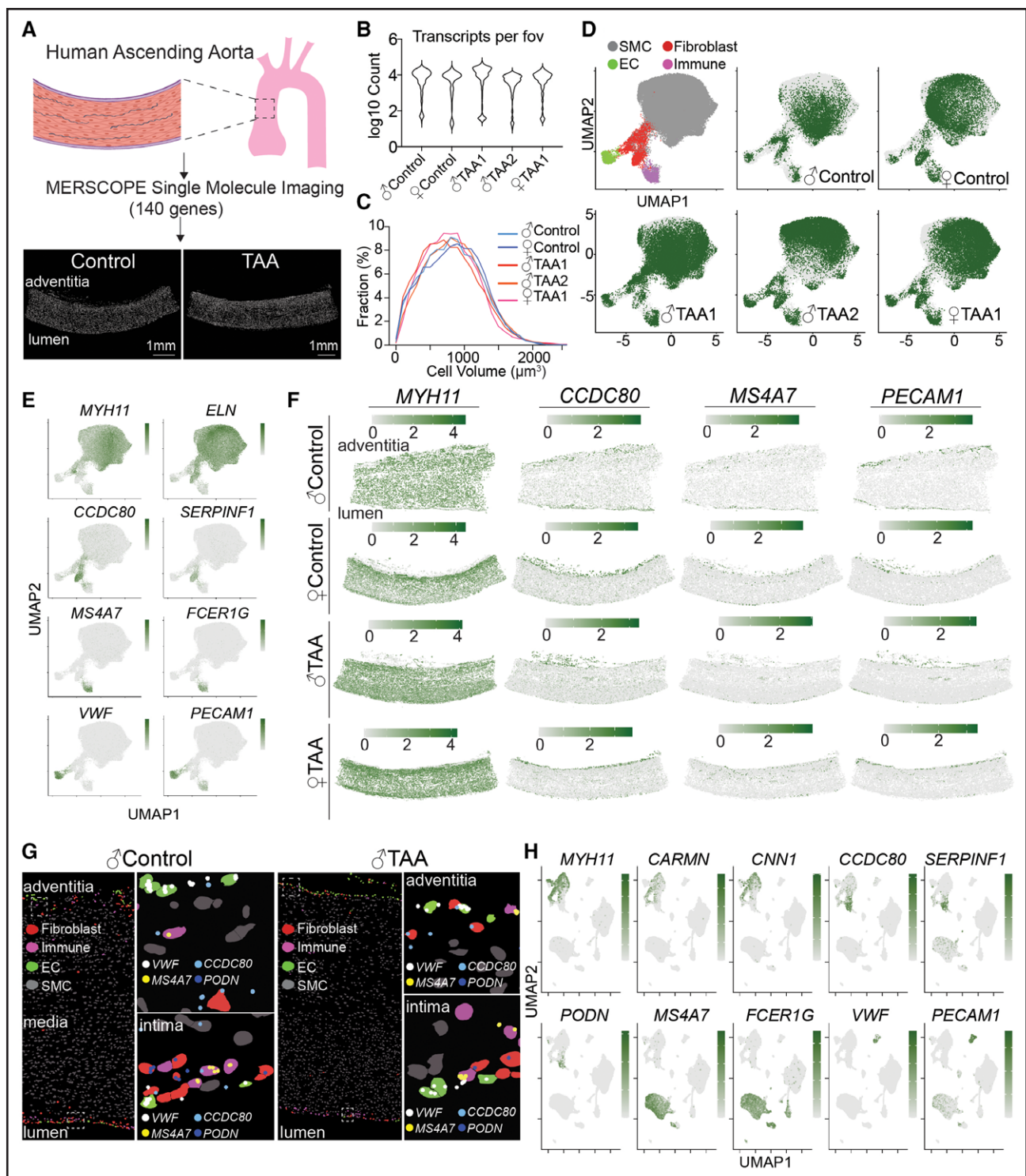
Figure 1. Single-molecule spatial transcriptomics of aneurysmal human ascending aorta.
A, Experimental design showing MERSCOPE profiling of nonaneurysmal (control) and aneurysmal (TAA) human ascending aorta. The tissue samples were extracted from the greater curvature. **B**, Violin plots showing transcript/molecule counts per field of view (fov) in each sample. Each fov is 200 μm.^{2} **C**, The distribution of individual cell volumes in each sample after cell segmentation. **D**, Uniform Manifold Approximation and Projection (UMAP) visualization showing major cell clusters (smooth muscle cell [SMC] clusters constituting the aortic media in gray; fibroblast cluster in red; immune cell cluster in purple; endothelial cell (EC) cluster in green). Individual samples are highlighted in dark green on the merged data set. **E**, Expression of top cluster markers on UMAP visualizations. **F**, Spatially resolved normalized expression of cluster markers in each centroid across different samples. **G**, Spatial distribution of fibroblast and EC clusters in the aortic wall. Individual transcript positions are highlighted using enlarged circles. Dashed boxes indicate the focused areas. **H**, Expression of top MERSCOPE cluster markers on UMAP visualizations of Li et al. dataset (3 control and 6 TAA samples).[9]
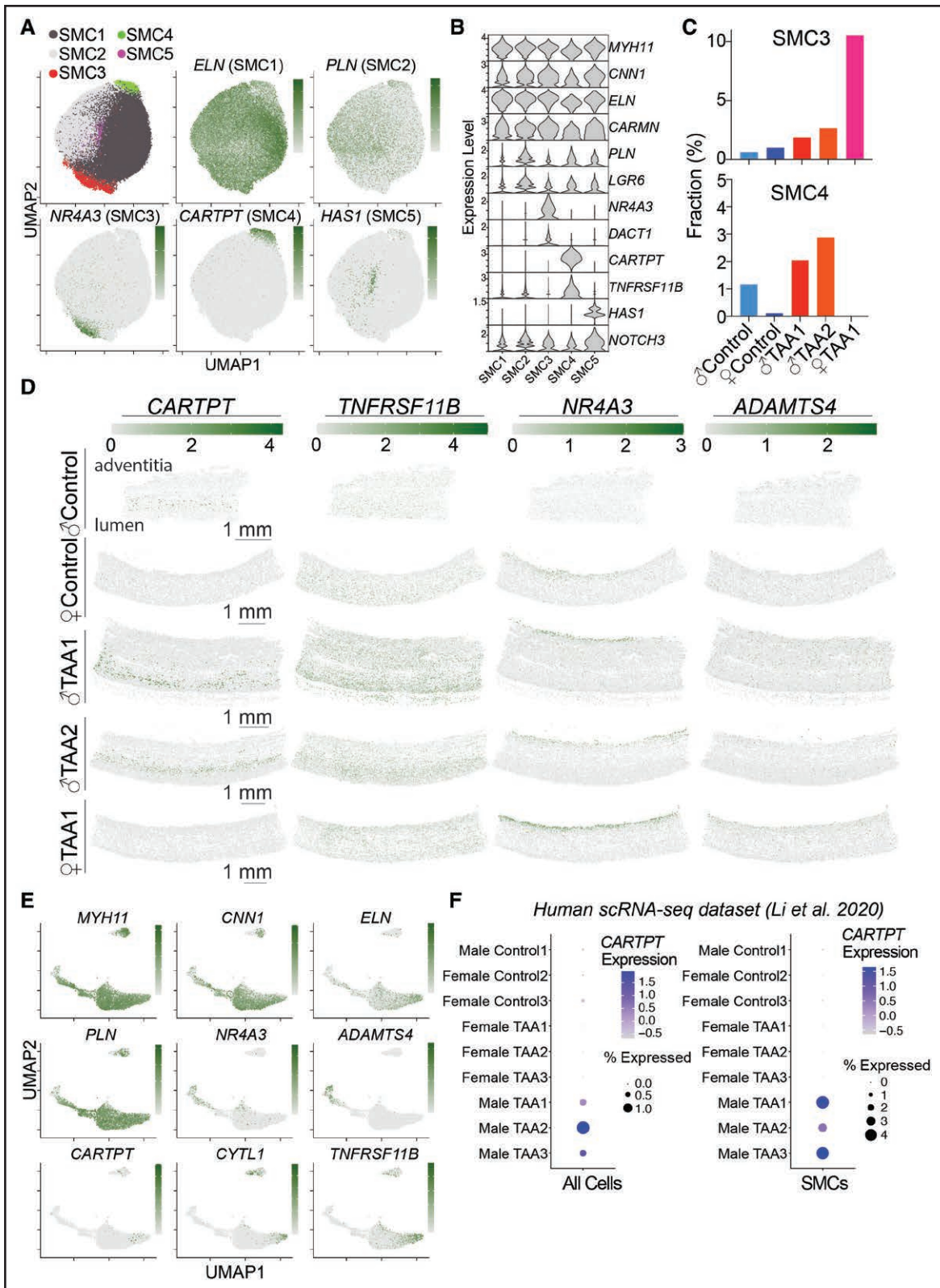
Figure 2. MERSCOPE Profiling reveals rare smooth muscle cell (SMC) subtypes.
A, Uniform Manifold Approximation and Projection (UMAP) visualization showing SMC subclusters. Expression levels of SMC subcluster markers are highlighted in green. **B**, Violin plots showing expression levels of enriched markers in SMC subclusters. **C**, Abundance of SMC3 and SMC4 in different samples normalized to the total SMC number in each sample. **D**, Spatially resolved normalized expression of SMC3 and SMC4 subcluster markers in SMCs across different samples. **E**, Expression levels of top MERSCOPE SMC subcluster markers in SMC clusters extracted from Li et al[9] data set. **F**, Dot plots showing *CARTPT*-expressing cell abundance and *CARTPT* expression levels among all cells or SMCs across 3 control and 6 thoracic aortic aneurysm (TAA) single-cell RNA-sequencing (scRNA-seq) samples.

a previously published dataset of human TAA single-cell RNA-sequencing.[9] Our major cluster markers for SMCs (myosin heavy chain 11 [*MYH11*], cardiac mesoderm enhancer-associated noncoding RNA [*CARMN*], calponin 1 [*CNN1*]), fibroblasts (*CCDC80*, *PODN*, *SERPINF1*), endothelial cells (*PECAM1*, *VWF*), and immune cells (*MS4A7*, *FCER1G*) labeled different cell groups in the merged data set while the markers for the same cell cluster showed colocalization to the same cell groups demonstrating the relevance of our cluster markers (Figure 1H).

MERSCOPE Profiling Reveals Rare SMC Subtypes

SMC defects are the main potentiators of TAA initiation and progression. To dissect SMC heterogeneity in the control and TAA samples, we performed SMC subclustering analysis, revealing 5 SMC subtypes (Figure 2A; Supplemental Excel Sheet 3). All SMC subtypes expressed SMC markers such as *MYH11*, *CNN1*, *CARMN,* and elastin (*ELN*) at variable levels (Figure 2B). SMC1 did not have any distinct markers within the 140 gene panel (Figure 2B). SMC2 was significantly enriched in phospholamban (*PLN*) and leucine-rich repeat−containing G protein-coupled receptor 6 (*LGR6*), while SMC5 had only one exclusive marker *HAS1* (*hyaluronan synthase 1*; Figure 2B; Supplemental Excel Sheet 3). Interestingly, we identified 2 rare SMC subtypes: SMC3 enriched in nuclear receptor subfamily 4 group A member 3 (*NR4A3*), ADAM metallopeptidase with thrombospondin type 1 motif 4 (*ADAMTS4*) and disheveled binding antagonist of beta-catenin 1 (*DACT1*); and SMC4 enriched in CART prepropeptide (*CARTPT*) and TNF receptor superfamily member 11b (*TNFRSF11B*; *P*-adj<0.001; Supplemental Excel Sheet 3). SMC3 and SMC4 also showed differential distribution among Control and TAA samples (Figure 2C). Interestingly, SMC4 was expanded in the TAA samples showing a male bias. Furthermore, differential gene expression analysis revealed signaling receptors *PLN* and *LGR6* were enriched in the Control SMCs, while notch receptor 3 (*NOTCH3*) and *TNFRSF11B* were higher in the TAA SMCs implying significant signaling changes in the TAA tissue (Figure S1A; Supplemental Excel Sheet 4).

Next, we plotted the spatially resolved expression of SMC3 and SMC4 markers on SMCs only across the control and TAA samples (Figure 2D). This revealed a restricted distribution of SMC3 markers such that *NR4A3* and *ADAMTS4* appeared more localized to the SMCs neighboring the adventitia (Figure 2D). Of note, the top *SMC3* markers such as *NR4A3* and *ADAMTS4* are significantly enriched in fibroblasts implying non-SMC origins of SMC3 (Supplemental Excel Sheet 2). Surprisingly, the most exclusive SMC4 marker; *CARTPT* transcript showed a spatially distinct distribution, labeling

a continuous layer of SMCs in the inner media of male TAA samples (Figures 2D; Figure S1B). The expression of fibroblast, immune cell, and endothelial cell cluster markers was very low in *CARTPT*-expressing SMC4 (Figure S1C). The other SMC4 marker; *TNFRSF11B*, is a more pervasive marker compared with *CARTPT* (Figure 2B) but still showed enrichment in the inner media of male TAA samples (Figure 2D).

To confirm the relevance of SMC3 and SMC4 in the human TAA scRNA-seq study, we examined their marker expression in SMCs from the Li et al[9] data set. *CARTPT* showed sparse labeling but overlapped with the more pervasive *TNFRSF11B* (Figure 2E) as well as another SMC4 marker; cytokine-like 1 (*CYTL1*; Supplemental Excel Sheet 3). Similarly, *NR4A3* and *ADAMTS4* appeared coexpressed in similar SMC populations (Figure 2E). More importantly, *CARTPT* expression showed a clear enrichment in 3 male TAA samples compared with 3 control and 3 female TAA samples consistent with our findings (Figure 2F). Additionally, we plotted the expression of *CARTPT* and more pervasive SMC4 markers (*TNFRSF11B* and *CYTL1*) on all single cells in the MERSCOPE and human scRNA-seq datasets. SMC4 markers had similar expression patterns with *CARTPT* being the most exclusive marker in both datasets (Figure S1D and S1E). Cumulatively, the human scRNA-seq data confirms the sex and TAA-based expression of *CARTPT* in the human aorta.

Human CART Is a Secreted Protein Enriched in Male Human TAA Tissue

Next, we investigated the spatial distribution of SMC3 and SMC4 among all SMCs across different samples. As expected, SMC3 were positioned near the adventitia with an enrichment in the female aneurysm sample, while SMC4 formed a continuous layer in the inner media (Figure 3A). Given the male bias and spatially distinct distribution of *CARTPT*, we focused on this gene and performed immunohistochemistry to confirm our findings at the protein level. Immunostainings on 2 control, 4 male TAA, and 4 female TAA samples revealed a clear enrichment of human CART in male TAA media with a distinguishable CART+ layer (Figures 3B; Figure S2A). Surprisingly, human CART is localized in the middle of the media and did not completely overlap with *CARTPT* mRNA expression positioned closer to intima suggesting the post-translational modification of CARTPT protein (Figures 2D and 3B).

CARTPT protein has several cleavage sites in its N-terminal and produces active peptides after site-specific cleavage.[32–35] Cleaved CART peptide can be released in the bloodstream in response to hypotensive stress.[36] Human CART peptides are also released in the cell culture medium.[32,35] Next, we asked whether human CART can be secreted by primary human aortic
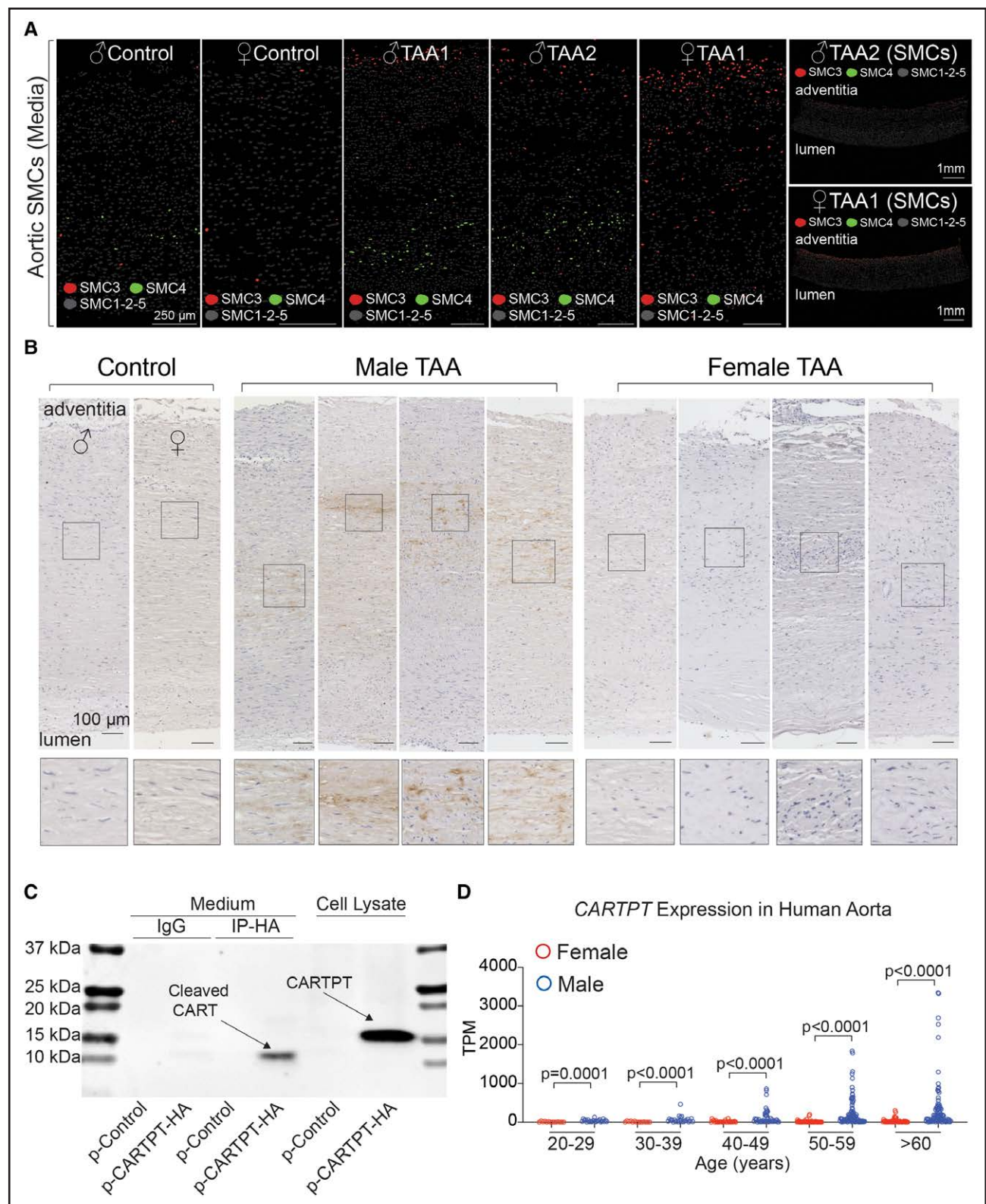
Figure 3. CART prepropeptide (*CARTPT*) expressing cells form a spatially distinct layer in male thoracic aortic aneurysm (TAA) samples.

A, Spatial distribution of smooth muscle cell (SMC) 3 (red) and SMC4 (green) in the aortic media. SMC1, SMC2, and SMC5 were colored in gray. **B**, Immunohistochemical stainings showing human CART labeling in male TAA samples. **Left**-to-**right**, TAA subjects ascending aorta measurements: male TAA (5.0 cm, same as ♂TAA1), male TAA (5.6 cm, same as ♂TAA2), male TAA (5.3 cm), male TAA (4.8 cm), female TAA (6.0 cm, same as ♀TAA1), female TAA (5.6 cm), female TAA (5.7 cm), female TAA (5.0 cm). **C**, Western blot showing cleaved human CART secretion in cell culture medium. Cell culture medium and lysate were collected from primary SMCs 2 days after transfection (*Continued*)

SMCs. To test this, primary SMCs were transfected with a vector containing human *CARTPT* with a C-terminal HA tag. Conditioned media was collected and subjected to coimmunoprecipitation using Protein G Magnetic Beads in conjunction with either IgG control or HA-targeting antibody. Western blot showed a larger band in cell lysate corresponding to the full-length CARTPT with an HA tag while we detected a smaller band in the cell culture medium coimmunoprecipitated with HA antibody suggesting that cleaved CART was released into the medium (Figure 3C).

To gain more insight into *CARTPT* regulation, we examined its expression among human aorta samples in An Integrating Platform of Age-Dependent Expression and Immune Profiles Across Human Tissues and The Genotype-Tissue Expression Project databases.[37] The An Integrating Platform of Age-Dependent Expression and Immune Profiles Across Human Tissues data confirmed the male enrichment of *CARTPT* in different age groups and near lack of *CARTPT* expression in female subjects (Figure 3D). We also noticed an age-dependent trend in *CARTPT* expression implying its regulation by vascular aging-related processes (Figure 3D). The Genotype-Tissue Expression Project data also confirmed the male enrichment of *CARTPT* in the human aorta and further suggests *CARTPT* enrichment in human aorta compared with most other tissues in the body (Figure S2B).

Human CART Promotes the Expression of Osteochondrogenic Transcription Factors in Human Primary SMCs

CARTPT expression is sensitive to stress and has been implicated in a stress-response system in mammalian brain.[32,38,39] To address its regulation in human aortic primary SMCs, we stimulated the cells using either a vehicle control of 10 ng/mL rhTNFα (recombinant human TNFα) or 25 µg/mL oxLDL. Interestingly, oxLDL treatment significantly increased *CARTPT* expression while rhTNFα treatment did not alter *CARTPT* level suggesting that a cardiovascular risk factor can induce *CARTPT* expression (Figure 4A). Next, we investigated the effects of human CART on SMC function. We transfected human aortic primary SMCs with human *CARTPT* vector, which increased *CARTPT* expression (Figure 4B). Canonical SMC contractility markers (*MYH11* and transgelin [*SM22*α]) were significantly downregulated only after 48 hours (Figure 4B). Given the upregulation of *CARTPT* mRNA and protein in male TAA tissue (Figures 2D and 3B), we also measured SMC phenotype switch markers including elastolytic enzyme matrix metallopeptidase

2 (*MMP2*) and key osteochondrogenic differentiation transcription factors; RUNX family transcription factor 2 (*RUNX2*) and msh homeobox 2 (*MSX2*).[40–45] All 3 markers were robustly upregulated in response to human *CARTPT* overexpression (Figure 4B).

Given that biologically active human CART is a secreted protein, we treated the primary SMCs with rhCART. Consistent with the overexpression experiment, the SMC contractility marker *SM22*α was reduced and *MYH11* showed a downregulation trend following 48 hours of rhCART treatment (Figure 4C). The expression of osteochondrogenic differentiation transcription factors *RUNX2* and *MSX2* were significantly upregulated (Figure 4C). Lastly, we performed real-time qPCRs to measure fibroblast marker expression (*CCDC80* and *SERPINF1*) after CARTPT overexpression and rhCART treatment. *CCDC80* and *SERPINF1* levels were either reduced or unaltered in both conditions suggesting that human CART does not promote fibroblast differentiation (Figure S3A). CART signaling has been shown to activate ERK signaling in different studies.[46–49] To further validate the effectiveness of rhCART treatment on human aortic primary SMCs, we treated the cells with rhCART for 24 hours and performed Western blots. Immunoblots revealed a robust elevation in p-ERK levels following rhCART treatment (Figure 4D).

Based on these results, human CART signaling appears to decrease SMC contractility markers and promote osteochondrogenic differentiation, which may eventually lead to calcium deposition in aorta. We examined calcification in our TAA samples by Alizarin red staining, commonly used to label calcium deposits.[50] The staining revealed variable levels of calcium deposition in male human TAA aortic media suggesting that male TAA samples were starting to calcify at the time of surgical resection (Figure 4E). Of note, 2 of the male TAA samples had significantly higher calcium deposition (Figure 4E). Strikingly, Alizarin red and human CART staining of male TAA samples label overlapping areas implying the link between human CART and medial calcification (Figures 3B and 4E). Additionally, to confirm the calcification in the male TAA samples, we performed Von Kossa stainings, which label mineralization and calcification in tissues.[50] This staining further validated the variable levels of mineralization/calcification in the aortic media of male TAA samples compared with the female TAA samples (Figure S3B).

DISCUSSION

This study demonstrates the feasibility of single-cell transcriptome imaging in uncovering aortic heterogeneity,

Figure 3 Continued. with p-CMV3-human CARTPT-HA. Human CART immunoprecipitation in cell culture medium was performed using an anti-HA antibody. **D**, *CARTPT* expression values (transcript per million [TPM]) in age-matched male and female human aorta samples downloaded from An Integrating Platform of Age-Dependent Expression and Immune Profiles Across Human Tissues Database (Mann-Whitney *U* test).
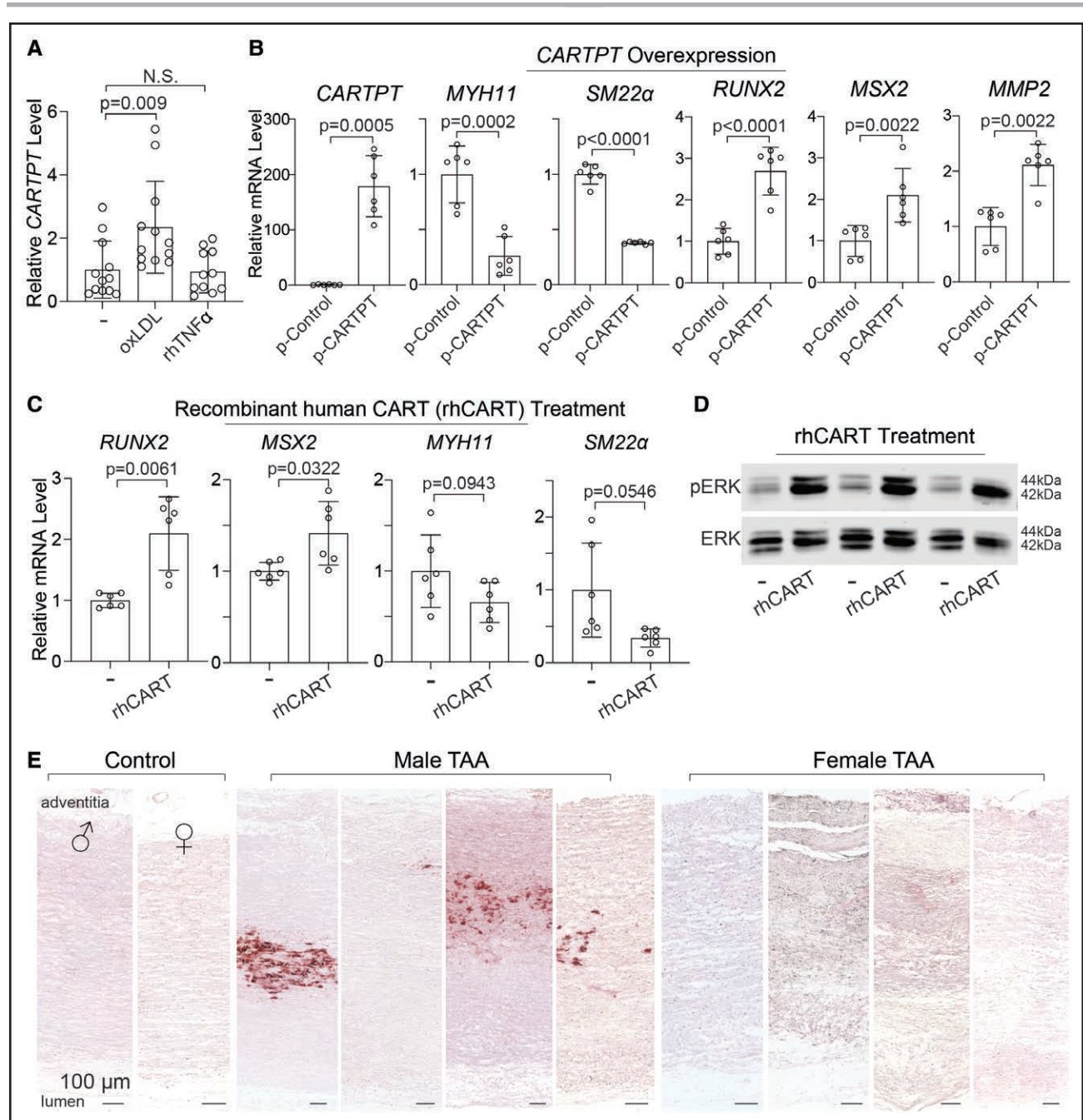
Figure 4. Human CART promotes the expression of osteochondrogenic transcription factors in smooth muscle cells (SMCs).
A, Relative *CARTPT* expression in untreated (n=12), oxLDL (oxidized low-density lipoprotein)-treated (n=12), and human TNFα (tumor necrosis factor)-treated (n=11) primary SMCs (Kruskal-Wallis test with Dunn multiple comparisons test). **B**, Relative expression of SMC markers, osteochondrogenic transcription factors, and *MMP2* after *CARTPT* overexpression in primary SMCs (n=6; unpaired *t* test with Welch correction for *CARTPT* and S*M22α* [*TAGLN*]; unpaired *t* test for *MYH11* and *RUNX2*; Mann-Whitney *U* test for *MSX2* and *MMP2*). **C**, Relative expression of SMC markers and osteochondrogenic transcription factors after rhCART (recombinant human CART) treatment of primary SMCs for 48 hours (n=6, unpaired *t* test with Welch correction for *RUNX2*, *MSX2,* and S*M22α*; unpaired *t* test for *MYH11*). **D**, Western blot showing ERK phosphorylation after rhCART treatment for 24 hours (n=3). **E**, Alizarin red staining showing variable medial calcium deposition in male thoracic aortic aneurysm (TAA) samples. rhTNFα indicates recombinant human TNF-alpha.

leading to the discovery of a spatially distinct *CARTPT*-expressing SMC subtype in male samples likely critical for medial calcification of the thoracic aorta. Unusually high extracellular matrix composition of the human aorta prevents reliable tissue dissociation. Suboptimal

cell dissociation can induce gene expression changes in individual cells and alter compositional profiles of different cell populations.[7] Although currently limited by the throughput, here, we show that in situ hybridization–based spatial profiling strategies including MERFISH

represent a powerful alternative to identify tissue-resident cell types in the human aorta and reveal their heterogeneity.

TAAs are more common in men but TAA growth and outcomes are worse in women for unknown reasons.[51,52] Similarly, abdominal aortic aneurysm is less frequent in female population but grows more aggressively than male abdominal aortic aneurysm with a higher risk of aortic rupture.[53,54] Our data reveals a robust enrichment of *CARTPT* expression in the male samples (Figures 2C and 2D and 3B), which we confirmed using other single-cell and bulk human aorta gene expression datasets (Figures 2F and 3D; Figure S2B). We propose that CART signaling promotes osteochondrogenic switch of aortic SMCs in male TAA tissue, eventually leading to medial calcification (Figure 4A through 4E; Figure S3B). Although thoracic and abdominal aortic calcification have been associated with higher cardiovascular and overall mortality, it is not clear whether calcification directly contributes to these adverse outcomes or is a consequence of underlying cardiovascular complications.[55] In fact, some studies suggest that aortic calcification stabilizes the aortic wall and slows down aortic aneurysm expansion, likely due to arterial stiffening.[56,57] It remains to be determined whether CART signaling–induced osteochondrogenic differentiation contributes to TAA formation or is protective against aggressive aortic dilation, dissection, and rupture in male patients with TAA.

In several vascular disease models including aortic aneurysms, a subset of preexisting SMCs can change their identity and undergo clonal expansion.[58] Osteoblast-like SMC differentiation has also been documented in the aging aorta.[59–62] *NR4A3*-enriched SMC3 are positioned near the adventitia, while *CARTPT*-enriched SMC4 are more abundant in the inner media suggesting that SMC3 and SMC4 likely originate from different aortic cell pools (Figure 3A). Our MERSCOPE data and the analysis of a previous human TAA scRNA-seq study demonstrate the emergence and expansion of *CARTPT*+ SMCs in male TAA tissue; however, the in vivo molecular triggers underlying this sex discrepancy are unknown. Although genetic predisposition plays a dominant role in TAA compared with abdominal aortic aneurysm, a significant portion of patients with TAA do not have a family history of the disease.[8] Causes of nonfamilial TAA remain to be determined.[63] Histologically determined atherosclerosis is observed in sporadic TAA cases and is associated with increased aortic media degeneration.[64] Our data suggests that oxLDL can induce *CARTPT* expression implying an atherosclerotic process in *CARTPT* regulation (Figure 4A). However, this finding does not suggest a link between atherosclerosis and male TAA as we currently do not know whether *CARTPT*-expressing SMCs contribute to TAA formation.

A limitation of MERSCOPE profiling approach is the number of genes that can be assayed. One hundred forty genes are undoubtedly insufficient to capture aortic heterogeneity, and inclusion of additional genes will likely reveal the full complexity of end-stage TAA tissue using the method described here. In addition, we were limited by our sample size. The analysis of the large An Integrating Platform of Age-Dependent Expression and Immune Profiles Across Human Tissues database shows *CARTPT* expression in a small number of aged female samples, albeit with lower levels and frequency compared with aged male samples (Figure 3D). Inclusion of female TAA subjects with medial calcification and male TAA subjects without medial calcification could also shed light on sex differences in *CARTPT* regulation. Despite these limitations, our study is a first step towards a high-resolution spatial cell ontology of the human aorta, and will be instrumental in defining actionable cell types and signaling pathways in human TAA tissue.

ARTICLE INFORMATION

Disclosures
D. Mizrak is a coinventor on a patent application related to microwell technology for single-cell sequencing that was filed by Columbia University. The other authors report no conflicts.

Supplemental Material
Figures S1–S3
Table S1
Major Resources Table
Supplemental Excel Sheets 1–4

REFERENCES

1. MacFarlane EG, Parker SJ, Shin JY, Kang BE, Ziegler SG, Creamer TJ, Bagirzadeh R, Bedja D, Chen Y, Calderon JF, et al. Lineage-specific events underlie aortic root aneurysm pathogenesis in Loeys-Dietz syndrome. *J Clin Invest.* 2019;129:659–675. doi: 10.1172/JCI123547

2. Pedroza AJ, Dalal AR, Shad R, Yokoyama N, Nakamura K, Cheng P, Wirka RC, Mitchel O, Baiocchi M, Hiesinger W, et al. Embryologic origin influences smooth muscle cell phenotypic modulation signatures in murine Marfan syndrome aortic aneurysm. *Arterioscler Thromb Vasc Biol.* 2022;42:1154–1168. doi: 10.1161/ATVBAHA.122.317381

3. Sawada H, Katsumata Y, Higashi H, Zhang C, Li Y, Morgan S, Lee LH, Singh SA, Chen JZ, Franklin MK, et al. Second heart field-derived cells

contribute to angiotensin II–mediated ascending aortopathies. *Circulation.* 2022;145:987–1001. doi: 10.1161/CIRCULATIONAHA.121.058173

4. Sawada H, Rateri DL, Moorleghen JJ, Majesky MW, Daugherty A. Smooth muscle cells derived from second heart field and cardiac neural crest reside in spatially distinct domains in the media of the ascending aorta-brief report. *Arterioscler Thromb Vasc Biol.* 2017;37:1722–1726. doi: 10.1161/ATVBAHA.117.309599

5. Shen M, Quertermous T, Fischbein MP, Wu JC. Generation of vascular smooth muscle cells from induced pluripotent stem cells: methods, applications, and considerations. *Circ Res.* 2021;128:670–686. doi: 10.1161/CIRCRESAHA.120.318049

6. Zhou D, Feng H, Yang Y, Huang T, Qiu P, Zhang C, Olsen TR, Zhang J, Chen YE, Mizrak D, et al. hiPSC modeling of lineage-specific smooth muscle cell defects caused by TGFBR1A230T variant, and its therapeutic implications for Loeys-Dietz syndrome . *Circulation.* 2021;144:1145–1159. doi: 10.1161/CIRCULATIONAHA.121.054744

7. Mizrak D, Feng H, Yang B. Dissecting the heterogeneity of human thoracic aortic aneurysms using single-cell transcriptomics. *Arterioscler Thromb Vasc Biol.* 2022;42:919–930. doi: 10.1161/ATVBAHA.122.317484

8. Pinard A, Jones GT, Milewicz DM. Genetics of thoracic and abdominal aortic diseases. *Circ Res.* 2019;124:588–606. doi: 10.1161/CIRCRESAHA.118.312436

9. Li Y, Ren P, Dawson A, Vasquez HG, Ageedi W, Zhang C, Luo W, Chen R, Li Y, Kim S, et al. Single-cell transcriptome analysis reveals dynamic cell populations and differential gene expression patterns in control and aneurysmal human aortic tissue. *Circulation.* 2020;142:1374–1388. doi: 10.1161/CIRCULATIONAHA.120.046528

10. Dawson A, Li Y, Li Y, Ren P, Vasquez HG, Zhang C, Rebello KR, Ageedi W, Azares AR, Mattar AB, et al. Single-cell analysis of aneurysmal aortic tissue in patients with Marfan syndrome reveals dysfunctional TGF-beta signaling. *Genes (Basel).* 2021;13:95. doi: 10.3390/genes13010095

11. Pedroza AJ, Tashima Y, Shad R, Cheng P, Wirka R, Churovich S, Nakamura K, Yokoyama N, Cui JZ, Iosef C, et al. Single-cell transcriptomic profiling of vascular smooth muscle cell phenotype modulation in Marfan syndrome aortic aneurysm. *Arterioscler Thromb Vasc Biol.* 2020;40:2195–2211. doi: 10.1161/ATVBAHA.120.314670

12. Zhang M, Eichhorn SW, Zingg B, Yao Z, Cotter K, Zeng H, Dong H, Zhuang X. Spatially resolved cell atlas of the mouse primary motor cortex by merfish. *Nature.* 2021;598:137–143. doi: 10.1038/s41586-021-03705-x

13. Hao Y, Hao S, Andersen-Nissen E, Mauck WM 3rd, Zheng S, Butler A, Lee MJ, Wilk AJ, Darby C, Zager M, et al. Integrated analysis of multimodal single-cell data. *Cell.* 2021;184:3573–3587.e29. doi: 10.1016/j.cell.2021.04.048

14. Wang Y, Hu J, Jiao J, Liu Z, Zhou Z, Zhao C, Chang LJ, Chen YE, Ma PX, Yang B. Engineering vascular tissue with functional smooth muscle cells derived from human iPS cells and nanofibrous scaffolds. *Biomaterials.* 2014;35:8960–8969. doi: 10.1016/j.biomaterials.2014.07.011

15. Wang L, Qiu P, Jiao J, Hirai H, Xiong W, Zhang J, Zhu T, Ma PX, Chen YE, Yang B. Yes-associated protein inhibits transcription of myocardin and attenuates differentiation of vascular smooth muscle cell from cardiovascular progenitor cell lineage. *Stem Cells.* 2017;35:351–361. doi: 10.1002/stem.2484

16. Guo DC, Gong L, Regalado ES, Santos-Cortez RL, Zhao R, Cai B, Veeraraghavan S, Prakash SK, Johnson RJ, Muilenburg A, et al; GenTAC Investigators, National Heart, Lung, and Blood Institute Go Exome Sequencing Project. MAT2A mutations predispose individuals to thoracic aortic aneurysms. *Am J Hum Genet.* 2015;96:170–177. doi: 10.1016/j.ajhg.2014.11.015

17. Isselbacher EM, Lino Cardenas CL, Lindsay ME. Hereditary influence in thoracic aortic aneurysm and dissection. *Circulation.* 2016;133:2516–2528. doi: 10.1161/CIRCULATIONAHA.116.009762

18. Gould RA, Aziz H, Woods CE, Seman-Senderos MA, Sparks E, Preuss C, Wunnemann F, Bedja D, Moats CR, McClymont SA, et al; Baylor-Hopkins Center for Mendelian Genomics. Robo4 variants predispose individuals to bicuspid aortic valve and thoracic aortic aneurysm. *Nat Genet.* 2019;51:42–50. doi: 10.1038/s41588-018-0265-y

19. Inamoto S, Kwartler CS, Lafont AL, Liang YY, Fadulu VT, Duraisamy S, Willing M, Estrera A, Safi H, Hannibal MC, et al. TGFBR2 mutations alter smooth muscle cell phenotype and predispose to thoracic aortic aneurysms and dissections. *Cardiovasc Res.* 2010;88:520–529. doi: 10.1093/cvr/cvq230

20. Koenig SN, LaHaye S, Feller JD, Rowland P, Hor KN, Trask AJ, Janssen PM, Radtke F, Lilly B, Garg V. Notch1 haploinsufficiency causes ascending aortic aneurysms in mice. *JCI Insight.* 2017;2:e91353. doi: 10.1172/jci.insight.91353

21. Luyckx I, MacCarrick G, Kempers M, Meester J, Geryl C, Rombouts O, Peeters N, Claes C, Boeckx N, Sakalihasan N, et al. Confirmation of the role of pathogenic SMAD6 variants in bicuspid aortic valve-related aortopathy. *Eur J Hum Genet.* 2019;27:1044–1053. doi: 10.1038/s41431-019-0363-z

22. Rodrigues Bento J, Meester J, Luyckx I, Peeters S, Verstraeten A, Loeys B. The genetics and typical traits of thoracic aortic aneurysm and dissection. *Annu Rev Genomics Hum Genet.* 2022;23:223–253. doi: 10.1146/annurev-genom-111521-104455

23. Zhao G, Lu H, Chang Z, Zhao Y, Zhu T, Chang L, Guo Y, Garcia-Barrio MT, Chen YE, Zhang J. Single-cell RNA sequencing reveals the cellular heterogeneity of aneurysmal infrarenal abdominal aorta. *Cardiovasc Res.* 2021;117:1402–1416. doi: 10.1093/cvr/cvaa214

24. Lu H, Sun J, Liang W, Chang Z, Rom O, Zhao Y, Zhao G, Xiong W, Wang H, Zhu T, et al. Cyclodextrin prevents abdominal aortic aneurysm via activation of vascular smooth muscle cell transcription factor EB. *Circulation.* 2020;142:483–498. doi: 10.1161/CIRCULATIONAHA.119.044803

25. Roychowdhury T, Lu H, Hornsby WE, Crone B, Wang GT, Guo DC, Sendamarai AK, Devineni P, Lin M, Zhou W, et al; VA Million Veteran Program. Regulatory variants in tcf7l2 are associated with thoracic aortic aneurysm. *Am J Hum Genet.* 2021;108:1578–1589. doi: 10.1016/j.ajhg.2021.06.016

26. Klarin D, Verma SS, Judy R, Dikilitas O, Wolford BN, Paranjpe I, Levin MG, Pan C, Tcheandjieu C, Spin JM, et al; Veterans Affairs Million Veteran Program†. Genetic architecture of abdominal aortic aneurysm in the million veteran program. *Circulation.* 2020;142:1633–1646. doi: 10.1161/CIRCULATIONAHA.120.047544

27. Wang Z, Zhao X, Zhao G, Guo Y, Lu H, Mu W, Zhong J, Garcia-Barrio M, Zhang J, Chen YE, et al. PRDM16 deficiency in vascular smooth muscle cells aggravates abdominal aortic aneurysm. *JCI Insight.* 2023;8:e167041. doi: 10.1172/jci.insight.167041

28. Chang Z, Zhao G, Zhao Y, Lu H, Xiong W, Liang W, Sun J, Wang H, Zhu T, Rom O, et al. BAF60A deficiency in vascular smooth muscle cells prevents abdominal aortic aneurysm by reducing inflammation and extracellular matrix degradation. *Arterioscler Thromb Vasc Biol.* 2020;40:2494–2507. doi: 10.1161/ATVBAHA.120.314955

29. Zhao G, Zhao Y, Lu H, Chang Z, Liu H, Wang H, Liang W, Liu Y, Zhu T, Rom O, et al. Baf60c prevents abdominal aortic aneurysm formation through epigenetic control of vascular smooth muscle cell homeostasis. *J Clin Invest.* 2022;132:e158309. doi: 10.1172/JCI158309

30. Canes L, Marti-Pamies I, Ballester-Servera C, Alonso J, Serrano E, Briones AM, Rodriguez C, Martinez-Gonzalez J. High NOR-1 (neuron-derived orphan receptor 1) expression strengthens the vascular wall response to angiotensin II leading to aneurysm formation in mice. *Hypertension.* 2021;77:557–570. doi: 10.1161/HYPERTENSIONAHA.120.16078

31. Ren P, Hughes M, Krishnamoorthy S, Zou S, Zhang L, Wu D, Zhang C, Curci JA, Coselli JS, Milewicz DM, et al. Critical role of ADAMTS-4 in the development of sporadic aortic aneurysm and dissection in mice. *Sci Rep.* 2017;7:12351. doi: 10.1038/s41598-017-12248-z

32. Rogge G, Jones D, Hubert GW, Lin Y, Kuhar MJ. Cart peptides: regulators of body weight, reward and other functions. *Nat Rev Neurosci.* 2008;9:747–758. doi: 10.1038/nrn2493

33. Thim L, Kristensen P, Nielsen PF, Wulff BS, Clausen JT. Tissue-specific processing of cocaine- and amphetamine-regulated transcript peptides in the rat. *Proc Natl Acad Sci U S A.* 1999;96:2722–2727. doi: 10.1073/pnas.96.6.2722

34. Dey A, Xhu X, Carroll R, Turck CW, Stein J, Steiner DF. Biological processing of the cocaine and amphetamine-regulated transcript precursors by prohormone convertases, pc2 and pc1/3. *J Biol Chem.* 2003;278:15007–15014. doi: 10.1074/jbc.M212128200

35. Yanik T, Dominguez G, Kuhar MJ, Del Giudice EM, Loh YP. The Leu34phe ProCART mutation leads to cocaine- and amphetamine-regulated transcript (CART) deficiency: a possible cause for obesity in humans. *Endocrinology.* 2006;147:39–43. doi: 10.1210/en.2005-0812

36. Larsen PJ, Seier V, Fink-Jensen A, Holst JJ, Warberg J, Vrang N. Cocaine- and amphetamine-regulated transcript is present in hypothalamic neuroendocrine neurones and is released to the hypothalamic-pituitary portal circuit. *J Neuroendocrinol.* 2003;15:219–226. doi: 10.1046/j.1365-2826.2003.00960.x

37. Liu X, Chen W, Fang Y, Yang S, Chang L, Chen X, Ye H, Tang X, Zhong S, Zhang W, et al. ADEIP: An integrated platform of age-dependent expression and immune profiles across human tissues. *Brief Bioinform.* 2021;22:bbab274. doi: 10.1093/bib/bbab274

38. Hunter RG, Bellani R, Bloss E, Costa A, Romeo RD, McEwen BS. Regulation of CART mRNA by stress and corticosteroids in the hippocampus and amygdala. *Brain Res.* 2007;1152:234–240. doi: 10.1016/j.brainres.2007.03.042

39. Stanley SA, Small CJ, Murphy KG, Rayes E, Abbott CR, Seal LJ, Morgan DG, Sunter D, Dakin CL, Kim MS, et al. Actions of cocaine- and

amphetamine-regulated transcript (CART) peptide on regulation of appetite and hypothalamo-pituitary axes in vitro and in vivo in male rats. *Brain Res*. 2001;893:186–194. doi: 10.1016/s0006-8993(00)03312-6

40. Petsophonsakul P, Furmanik M, Forsythe R, Dweck M, Schurink GW, Natour E, Reutelingsperger C, Jacobs M, Mees B, Schurgers L. Role of vascular smooth muscle cell phenotypic switching and calcification in aortic aneurysm formation. *Arterioscler Thromb Vasc Biol*. 2019;39:1351–1368. doi: 10.1161/ATVBAHA.119.312787

41. Sun Y, Byon CH, Yuan K, Chen J, Mao X, Heath JM, Javed A, Zhang K, Anderson PG, Chen Y. Smooth muscle cell-specific RUNX2 deficiency inhibits vascular calcification. *Circ Res*. 2012;111:543–552. doi: 10.1161/CIRCRESAHA.112.267237

42. Cheng SL, Shao JS, Charlton-Kachigian N, Loewy AP, Towler DA. MSX2 promotes osteogenesis and suppresses adipogenic differentiation of multipotent mesenchymal progenitors. *J Biol Chem*. 2003;278:45969–45977. doi: 10.1074/jbc.M306972200

43. Risinger GM Jr, Hunt TS, Updike DL, Bullen EC, Howard EW. Matrix metalloproteinase-2 expression by vascular smooth muscle cells is mediated by both stimulatory and inhibitory signals in response to growth factors. *J Biol Chem*. 2006;281:25915–25925. doi: 10.1074/jbc.M513513200

44. Ailawadi G, Moehle CW, Pei H, Walton SP, Yang Z, Kron IL, Lau CL, Owens GK. Smooth muscle phenotypic modulation is an early event in aortic aneurysms. *J Thorac Cardiovasc Surg*. 2009;138:1392–1399. doi: 10.1016/j.jtcvs.2009.07.075

45. Speer MY, Li X, Hiremath PG, Giachelli CM. RUNX2/CBFA1, but not loss of myocardin, is required for smooth muscle cell lineage reprogramming toward osteochondrogenesis. *J Cell Biochem*. 2010;110:935–947. doi: 10.1002/jcb.22607

46. Yosten GL, Harada CM, Haddock C, Giancotti LA, Kolar GR, Patel R, Guo C, Chen Z, Zhang J, Doyle TM, et al. GPR160 de-orphanization reveals critical roles in neuropathic pain in rodents. *J Clin Invest*. 2020;130:2587–2592. doi: 10.1172/JCI133270

47. Lakatos A, Prinster S, Vicentic A, Hall RA, Kuhar MJ. Cocaine- and amphetamine-regulated transcript (CART) peptide activates the extracellular signal-regulated kinase (ERK) pathway in ATT20 cells via putative G-protein coupled receptors. *Neurosci Lett*. 2005;384:198–202. doi: 10.1016/j.neulet.2005.04.072

48. Owe-Larsson M, Pawlasek J, Piecha T, Sztokfisz-Ignasiak A, Pater M, Janiuk IR. The role of cocaine- and amphetamine-regulated transcript (CART) in cancer: a systematic review. *Int J Mol Sci*. 2023;24:9986. doi: 10.3390/ijms24129986

49. Somalwar AR, Choudhary AG, Sharma PR, B N, Sagarkar S, Sakharkar AJ, Subhedar NK, Kokare DM. Cocaine- and amphetamine-regulated transcript peptide (cart) induced reward behavior is mediated via $G_{i/o}$ dependent phosphorylation of PKA/ERK/CREB pathway. *Behav Brain Res*. 2018;348:9–21. doi: 10.1016/j.bbr.2018.03.035

50. Luo G, Ducy P, McKee MD, Pinero GJ, Loyer E, Behringer RR, Karsenty G. Spontaneous calcification of arteries and cartilage in mice lacking matrix Gla protein. *Nature*. 1997;386:78–81. doi: 10.1038/386078a0

51. Cheung K, Boodhwani M, Chan KL, Beauchesne L, Dick A, Coutinho T. Thoracic aortic aneurysm growth: Role of sex and aneurysm etiology. *J Am Heart Assoc*. 2017;6:e003792. doi: 10.1161/JAHA.116.003792

52. Voigt KR, Gokalp AL, Papageorgiou G, Bogers A, Takkenberg JJM, Mokhles MM, Bekkers JA. Male-female differences in ascending aortic aneurysm surgery: 25-year single center results. *Semin Thorac Cardiovasc Surg*. 2023;35:300–308.

53. Malayala SV, Raza A, Vanaparthy R. Gender-based differences in abdominal aortic aneurysm rupture: a retrospective study. *J Clin Med Res*. 2020;12:794–802. doi: 10.14740/jocmr4376

54. Hannawa KK, Eliason JL, Upchurch GR Jr. Gender differences in abdominal aortic aneurysms. *Vascular*. 2009;17:S30–S39. doi: 10.2310/6670.2008.00092

55. Chowdhury MM, Zielinski LP, Sun JJ, Lambracos S, Boyle JR, Harrison SC, Rudd JHF, Coughlin PA. Editor's choice - calcification of thoracic and abdominal aneurysms is associated with mortality and morbidity. *Eur J Vasc Endovasc Surg*. 2018;55:101–108. doi: 10.1016/j.ejvs.2017.11.007

56. Klopf J, Fuchs L, Schernthaner R, Domenig CM, Gollackner B, Brostjan C, Neumayer C, Eilenberg W. The prognostic impact of vascular calcification on abdominal aortic aneurysm progression. *J Vasc Surg*. 2022;75:1926–1934. doi: 10.1016/j.jvs.2021.11.062

57. Nakayama A, Morita H, Hayashi N, Nomura Y, Hoshina K, Shigematsu K, Ohtsu H, Miyata T, Komuro I. Inverse correlation between calcium accumulation and the expansion rate of abdominal aortic aneurysms. *Circ J*. 2016;80:332–339. doi: 10.1253/circj.CJ-15-1065

58. Clement M, Chappell J, Raffort J, Lareyre F, Vandestienne M, Taylor AL, Finigan A, Harrison J, Bennett MR, Bruneval P, et al. Vascular smooth muscle cell plasticity and autophagy in dissecting aortic aneurysms. *Arterioscler Thromb Vasc Biol*. 2019;39:1149–1159. doi: 10.1161/ATVBAHA.118.311727

59. Mammoto A, Matus K, Mammoto T. Extracellular matrix in aging aorta. *Front Cell Dev Biol*. 2022;10:822561. doi: 10.3389/fcell.2022.822561

60. Nakano-Kurimoto R, Ikeda K, Uraoka M, Nakagawa Y, Yutaka K, Koide M, Takahashi T, Matoba S, Yamada H, Okigaki M, et al. Replicative senescence of vascular smooth muscle cells enhances the calcification through initiating the osteoblastic transition. *Am J Physiol Heart Circ Physiol*. 2009;297:H1673–H1684. doi: 10.1152/ajpheart.00455.2009

61. Monk BA, George SJ. The effect of ageing on vascular smooth muscle cell behaviour--a mini-review. *Gerontology*. 2015;61:416–426. doi: 10.1159/000368576

62. Wang JC, Bennett M. Aging and atherosclerosis: Mechanisms, functional consequences, and potential therapeutics for cellular senescence. *Circ Res*. 2012;111:245–259. doi: 10.1161/CIRCRESAHA.111.261388

63. Shen YH, LeMaire SA. Molecular pathogenesis of genetic and sporadic aortic aneurysms and dissections. *Curr Probl Surg*. 2017;54:95–155. doi: 10.1067/j.cpsurg.2017.01.001

64. Albini PT, Segura AM, Liu G, Minard CG, Coselli JS, Milewicz DM, Shen YH, LeMaire SA. Advanced atherosclerosis is associated with increased medial degeneration in sporadic ascending aortic aneurysms. *Atherosclerosis*. 2014;232:361–368. doi: 10.1016/j.atherosclerosis.2013.10.035